

RESEARCH ARTICLE | JUNE 16 2022

Concept, design, and measurement methodology of a highly dynamic thin film dryer for experimental *in situ* drying manipulation

Martin Schugmann   ; Petra Foerst 

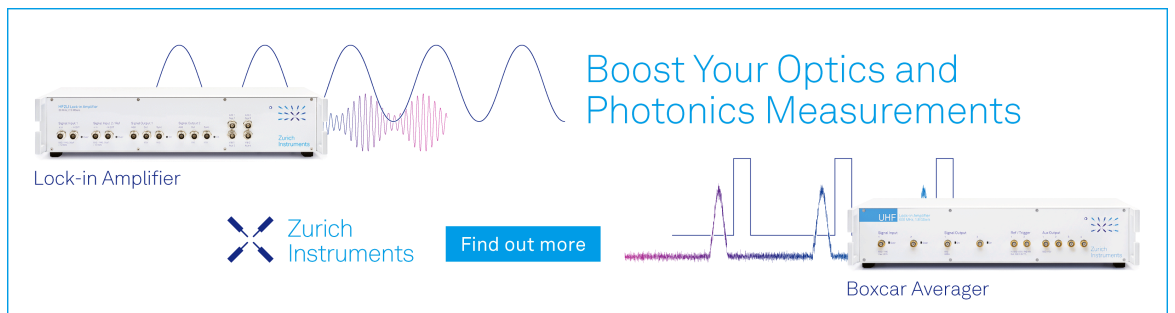


Rev. Sci. Instrum. 93, 065108 (2022)


<https://doi.org/10.1063/5.0083295>



Boost Your Optics and Photonics Measurements



Lock-in Amplifier

 Zurich Instruments

[Find out more](#)

Boxcar Averager

Concept, design, and measurement methodology of a highly dynamic thin film dryer for experimental *in situ* drying manipulation

Cite as: Rev. Sci. Instrum. 93, 065108 (2022); doi: 10.1063/5.0083295

Submitted: 23 December 2021 • Accepted: 17 May 2022 •

Published Online: 16 June 2022



View Online



Export Citation



CrossMark

Martin Schugmann^{a)}  and Petra Foerst 

AFFILIATIONS

Institute of Process Systems Engineering, Technical University of Munich, Gregor-Mendel-Straße 4, 85354 Freising, Germany

^{a)} Author to whom correspondence should be addressed: martin.schugmann@tum.de

ABSTRACT

This paper describes the technical setup and validation of a thin film drying device in which the conditions such as air temperature, relative humidity, and velocity can be controlled in the range of 20–200 °C, 0–1.5 m s⁻¹, and vapor mass flows up to 1200 g min⁻¹. For the first time, it is possible to perform *in situ* manipulation of the drying kinetic in a highly dynamic manner. The setup allows for a precise online determination of drying and rehydration kinetics; the recording of relevant process parameters such as air humidity, air and surface temperature; and the monitoring of optically observable material properties. The concept for rapid real-time changes in drying conditions is explained, and the constructive details are elucidated. Highly precise gravimetry by a proposed measurement methodology and simultaneously avoiding condensation during rapid parameter changes is accomplished. This is achieved by the combination of minimized thermal inertia of the system, air conditioning via carrier gas-free evaporation, and a highly responsive active insulation. The influence on the drying kinetics by temperature, humidity, and air velocity is shown with experiments on aqueous maltose solution, and the experimental precision is validated. The validation showed a high grade of accuracy regarding gravimetric determination with a maximum observed mass difference of 0.21% referring to the dried product. The dynamics of the setup under *in situ* changes in drying conditions is exemplified by further experiments. In addition, the presented setup for the first time enables the real time manipulation and observation of kinetically coupled processes such as crystallization behavior, morphology formation, or material degradation during drying. Therefore, it has important practical value for the development of efficient and energy-saving drying methods and products with specific, tailor-made properties.

© 2022 Author(s). All article content, except where otherwise noted, is licensed under a Creative Commons Attribution (CC BY) license (<http://creativecommons.org/licenses/by/4.0/>). <https://doi.org/10.1063/5.0083295>

I. INTRODUCTION

The convective drying process is an important unit operation in the food and pharmaceutical industries. Common technologies are spray drying, fluidized bed drying, or tray drying. Nevertheless, drying is a complex process due to simultaneous heat and mass transfer. The influence of the drying conditions on the product properties is and remains the scope of diverse, intensive research activities.^{1–7} Accurate knowledge and determination of drying kinetics are, therefore, essential to realize modeling approaches. Examples are upscaling efforts or the coupling of drying-related effects such as degradation, wall deposition, particle morphology, oxidation, or loss of valuable components such as amino acids and vitamins.^{3,6,8}

In addition, physical characteristics, such as crystallinity of sugar-rich products, can be influenced by the drying kinetics and have a major effect on the products post-drying stability or flowability during handling or storage.^{9–11}

In addition, often drying processes of foodstuffs or pharmaceuticals are carried out under predefined and constant conditions in regard to air humidity, airflow, and temperature, although control and adjustment of these parameters could specifically influence the product properties. By specifically and quickly changing the conditions, the drying kinetics and also the product temperature can be influenced at any stage of the drying process. These manipulations make it possible to specifically control kinetically coupled processes such as crystallization behavior, morphology formation,

or material degradation already during the drying process. Chen *et al.*, for instance, showed with experiments on walnut drying at constant and step-down temperature (from 65 to 43 °C after 2 h of drying conditions) that the drying time could be reduced by 40% while obtaining similar quality and better shelf life in the dried products.¹² Woo *et al.* highlighted in their review on the *in situ* control of crystallization during spray drying that the key strategy is to manipulate the evaporation time to control the nucleation and growth of crystals or solid phase transition within dehydrating droplets. This can be done by controlling the drying rate within the spray dryer.¹³ Har *et al.* showed in this context that temperature differences of 20 °C (from 70 to 90 °C) are already decisive to noticeably influence the crystallization behavior.¹⁴ Woo *et al.* demonstrated in single droplet drying experiments that differences in the critical period of around 2 min lead to different crystallinity.¹⁵ Shakiba *et al.* showed with experiments on a counter-current spray dryer that lactose crystallinity could be altered via humidity injection (drying rate manipulation) within specific regions in the drying chamber.¹⁶ This author also stated that the stickiness behavior could be completely changed with a change in relative humidity between 40% and 80% with remaining conditions (80 °C; air velocity 0.30 m s⁻¹) unchanged.^{3,17} In addition, the kinetics of protein loss during thin film drying (TFD) in lactose rich dairy products can be altered by varying the drying conditions temperature and air velocity between 80 and 100 °C, respectively, 0.15 and 0.3 m s⁻¹.³ To conduct and observe *in situ* manipulations experimentally, dynamic changes of drying process parameters should be possible within the mentioned dimensions.

Common experimental approaches to assess the drying kinetics of pharmaceutical and food products can be divided into four main categories: (a) solid-supported droplets filament technique^{14,18,19} or immobilized droplets,^{20,21} (b) droplets in aerodynamic fields in falling towers, spray towers, or free-floating droplets,^{22,23} (c) acoustic levitation,^{24,25} and (d) thin film drying (TFD).^{3,26–28} Since drying concepts (b) and (c) have serious disadvantages regarding practicability and influence on the mass transport, the drying kinetics are often determined by (a) and (d), namely, by the drying of single drops on filaments and thin-layer drying. One advantage of experimental, convective TFD is that the mass and temperature of the film can be better monitored during drying, which is not possible during spray drying and more difficult during single-drop drying. In addition, the contribution of heat input/conduction is not negligible for small droplet sizes.⁴ In addition, compared to single-droplet drying, significantly more product is available for subsequent property and surface analyses, e.g., composition and crystallinity. Furthermore, *in situ* observation of processes such as morphology development, diffusion measurements, or crystallization is simplified due to the defined sample area and flat surface.^{26,28,29}

In the following, existing thin-film devices are briefly described. Schmitz-Schug *et al.* used a thin film dryer for the determination of drying kinetics of skim milk. However, the setup had neither online gravimetry nor the possibility of contactless acquisition of the sample temperature or the variation of humidity, which can cause inaccuracies.³ Gomez-Narvaez described in detail the construction of a TFD setup with online gravimetry but without the possibility of air humidification, variable control during operation or continuous recording.²⁷ Räderer *et al.* used a TFD setup for drying experiments; however, the drying parameters cannot be changed during

experiments.²⁸ Furthermore, Li *et al.*, Both *et al.*, and Adhikari *et al.* described devices for isothermal, thin-film drying with dry air, however, without the possibility to change the humidity, air velocity, or temperature during drying.^{30–32}

Nevertheless, until now there is no description of an experimental setup for validated high-precision determination of the convective drying kinetics of thin films in which, on the one hand, an investigation is possible in a broad range of temperature, air velocity, and humidity and, on the other hand, these conditions can be changed quickly and in real-time. This paper makes a contribution in this direction and presents a TFD apparatus, its constructive details, function, and a measurement methodology for increased accuracy with respect to drying kinetics.

II. SETUP OF THE THIN FILM DRYING DEVICE

A. General specifications

The drying equipment presented here is expected to fulfill the task of convective drying and rehydrating thin films under defined environmental and flow conditions. The aim is to investigate the influence of the drying conditions on optically observable product properties of sugars and sugar-rich goods (e.g., browning, vitamin loss, or crystallization). Therefore, precise control of the air velocity, temperature, and relative humidity is necessary. To influence the drying kinetics *in situ* and control the property formation, it is necessary to be able to rapidly change these parameters. It should be possible to vary the parameters within the ranges elucidated in Sec. I and in a much shorter time frame than the drying time of typical TFD processes. Furthermore, the recording of the drying kinetics, images, and surface temperature should be enabled.

The present concept allows an operation within a wide range of conditions: The airflow rate can be controlled between a standard volume flow of 5 and 100 l min⁻¹, which leads to a flow velocity range between 0.08 and 1.5 m s⁻¹ for the present channel dimensions at temperatures up to 200 °C. Water mass flows of 20–1200 g h⁻¹ can be controlled resulting in a saturated airflow up to 100 °C at 0.5 m s⁻¹. Figure 1 specifies the range of maximum relative humidity depending on temperature and air velocity. At temperatures above 100 °C, drying manipulation can also take place by pure superheated vapor or vapor–air mixtures.

B. Constructive details

Figure 2 shows a sectional view through the drying channel of the setup at the sample site. The technical drawings and dimensions of the main parts are shown in the [supplementary material](#). The dryer duct, inlet, and outlet are milled from an AlMgPb alloy and have a wall thickness of 0.8 mm. The low wall thickness and use of a material with high thermal conductivity allows for minimized thermal inertia of the system and, thus, a fast response to temperature changes. The internal cross section of the duct is 18 × 60 mm², and the distance to the sample is 200 mm. An integrated frame structure gives the duct the required mechanical stability. The body is closed from the top with a lid. Measuring equipment (local air temperature, relative humidity) and windows for contactless surface temperature measurement or other optical techniques (Raman and UV–vis spectroscopy, polarized light imaging) are embedded in this lid. The duct inlet (length 181 mm, opening angle 17°) and

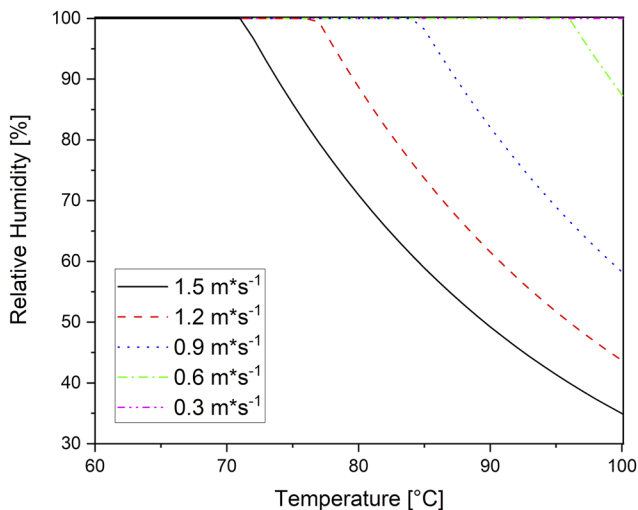


FIG. 1. Maximum relative humidity at different air velocities in the operating range up to boiling point. Above boiling point, superheated vapor (max. 1200 g h⁻¹) or air-vapor mixtures can be used up to a temperature of 200 °C.

outlet are screwed to stud bolts at the front and rear. The channel has an opening from below after the inlet section through which the sample rack projects into the channel without changing its cross section. This insert is equipped with holes through which the feet

of the rack (of slightly smaller diameter, gap distance of 0.5 mm) protrude. The sample platelet (52 × 52 × 1 mm³) rests on the rack. The cavity depth in the sample platelet was adapted to the dried film thickness so that the surface of the dried film lies in a plane with the edges. The average film thickness after drying on a test platelet was measured with a laser scanning microscope. In addition, the area between the isolation duct and the dryer duct is flushed with dry, temperature-controlled air to prevent condensation of humid air from escaping from the duct. The purge flow around the feet is adjusted with the help of orifice plates with variable permeability. Controlled purging prevents errors in weight measurement due to excessive flow or condensation and allows dynamic temperature or humidity changes and yet highly accurate gravimetry. The balance housing is additionally purged with an airflow of 20 ml min⁻¹ and ambient temperature. This eliminates systematic errors due to temperature or moisture fluctuations. The sample rack assembly (tripod) is fabricated out of PEEK (Polyether ether ketone) with thermal stability of >200 °C and low thermal conductivity, which prevents condensation. It is leviable via three M3 × 0.35 fine-pitch threaded pinpoint stands and secured by lock nuts in a socket. The pinpoint design minimizes heat dissipation via conduction and allows very accurate leveling for a constant thin film thickness. At the sample site, there is another opening on the side for inserting the platelet, which is closed by another insert with a glass window. For contactless temperature measurement, basis for precise gravimetry, an IR camera is installed above the top windows. Therefore, the observation takes place via two anti-reflective zinc selenide

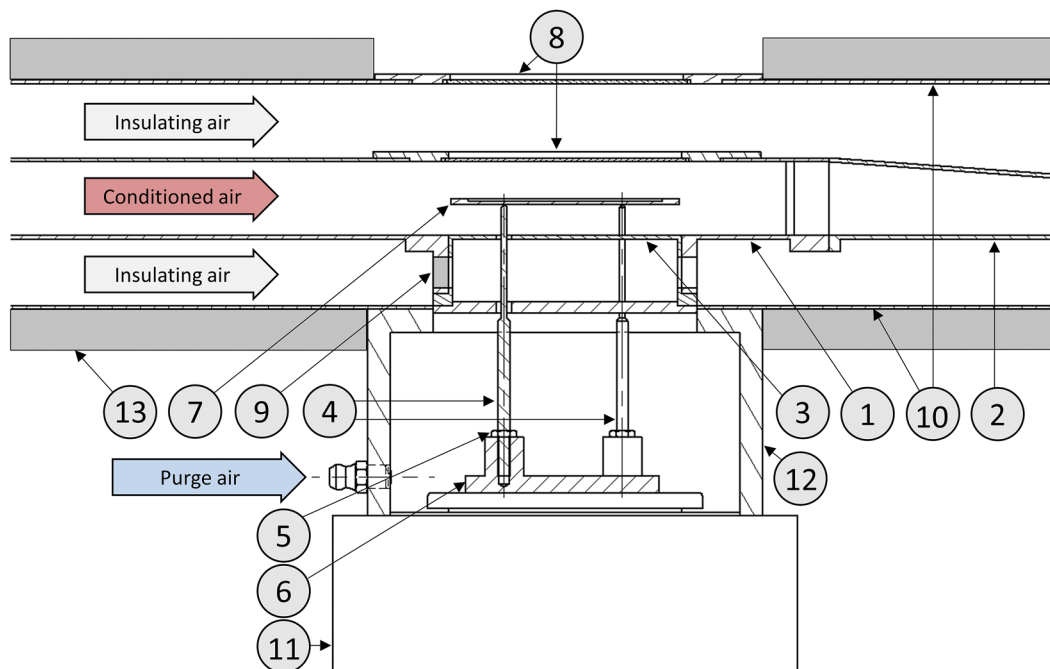


FIG. 2. Sectional view of the drying setup at the sample site: (1) dryer duct, (2) outlet, (3) insert for sample rack protrusion, (4) fine-pitch threaded pinpoint stands, (5) lock nut, (6) rack socket with inner thread, (7) sample platelet, (8) top windows for optical analytics, (9) adjustable orifice, (10) insulation duct, (11) precision balance, (12) purged balance housing, and (13) passive insulation. Measurement equipment for temperature, moisture, and optical analyses is not shown. The wall thicknesses and drill holes are not in scale for illustrative purposes.

windows. Side opening and window inserts do not affect the cross section. Figure 3 shows a perspective view of the setup's channel section assembly.

C. Air conditioning

A central requirement is the flexible and fast control of the humidity in a wide range in order to influence the drying kinetics in a highly dynamic manner. This setup uses a carrier gas-free direct evaporator, gas preheating, and a heated mixing chamber. Compared to bubbler systems or carrier gas spray evaporators, the apparatus effort is significantly higher but it decouples the gas flow, water flow, and outlet temperature parameters. As much or as little gas as desired can be mixed with the desired amount of pure steam, preheating can be used to enable condensation-free mixing of the two components and the heated mixing chamber ensures droplet-free operation. Due to the design-related minimal thermal masses of this concept of air supply, it shows high flexibility in comparison to other possible approaches of conditioned air supply such as bubbler systems or spray evaporators with regard to high temperature and/or humidity changes and was, therefore, chosen for the setup.

D. Process flow

The air is taken from the laboratory compressed air system (8 bars) and is cleaned via a compressed air dehumidifier and filter CT-1 (Drypoint; Beko Technologies GmbH; Germany), as seen in Fig. 4. A mass flow controlled (MFC) valve V-3 (El Flow Select; Bronkhorst B.V.; Netherlands) is used to control the mass flow of air. Deionized water is taken from reservoir B-1 with a 20 l volume. The mass flow is controlled by the MFC valve V-4 (mini-Cori-Flow; Bronkhorst B.V.; Netherlands). With the evaporator-mixer unit VM-1 (W 303b; Bronkhorst B.V.; Netherlands; maximum temperature 200 °C), the water is evaporated, mixed with pre-tempered, dry air, and then tempered to the exact setpoint. The conditioned air is directed into the drying channel TK-1 and flows over the sample inside it. The air velocity profile can be manipulated by the

additional installation of grids D-1 and D-2, which can be plugged in by the means of small vertical grooves in the ducts walls (see the drawing of the main duct in the [supplementary material](#)). During operation without a diffuser, the grooves can be covered by an insert so that the cross section of the flow does not change. The thin film, which is spread on a platelet with a cavity, is mounted on a sample carrier PT-1 coupled to a precision balance WIR-1 (Pioneer PX225e; Ohaus Europe GmbH; Switzerland; reproducibility 0.1 mg). In order to prevent condensation in the channel at simultaneously high temperature and humidity levels, the channel is surrounded by another channel through which insulating air of the same temperature flows, which is tempered by a hot air blower HE-1 (Hot wind Mistral 6; Leister AG; Switzerland) that can be controlled with respect to temperature and volume flow. The surrounding channel, in turn, is passively insulated with mineral wool to prevent heat loss. By means of active insulation, using temperature-controlled air, the power of the blower can be adapted very quickly to changing test requirements within an experiment, since air has low thermal inertia compared to liquid-controlled insulation. The evaporator-mixer unit VM-1 and the air temperature are controlled directly with the control valves V-3 and V-4. The air humidity can, thus, be controlled by adjusting the mass flow ratio of water and air and the temperature. The windows in the insulation duct and the actual drying duct are interchangeable for specific experimental questions. The surface temperature is measured contactless with the help of an infrared camera (FLIR A325sc; Teledyne FLIR LLC; Oregon/USA) through anti-reflective zinc selenide windows. Optically observable changes in the properties of the sample can be monitored through double anti-reflective quartz glass windows with a camera. The setup for monitoring either the optical properties of the whole sample area or its planar temperature profile is depicted in Fig. 3. The simultaneous measurement of temperature and optical changes is also possible; see the technical drawing in the [supplementary material](#). The air temperature is measured with two class-A PT 1000 temperature sensors TIR-1 and TIR-2 (RS Components GmbH; Germany) in front of and behind the sample. The relative humidity can be determined at two points in the channel via sleeves MIR-1 and 2 (Testo

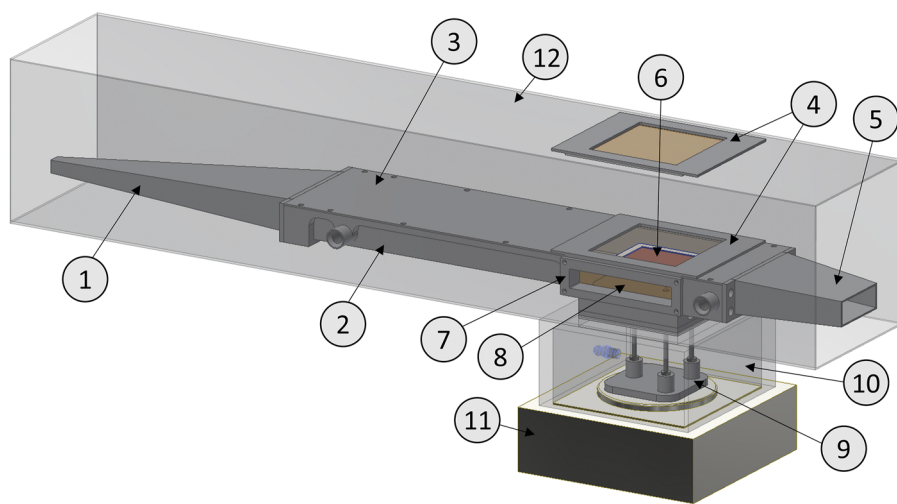


FIG. 3. Perspective view of the setup's channel section: (1) inlet, (2) dryer duct, (3) top lid, (4) top windows, (5) outlet, (6) sample platelet, (7) side door for sample insertion, (8) window for illumination and/or position control of the sample, (9) sample rack, (10) balance housing, (11) precision balance, and (12) insulation duct. Measurement equipment and passive insulation are not shown.

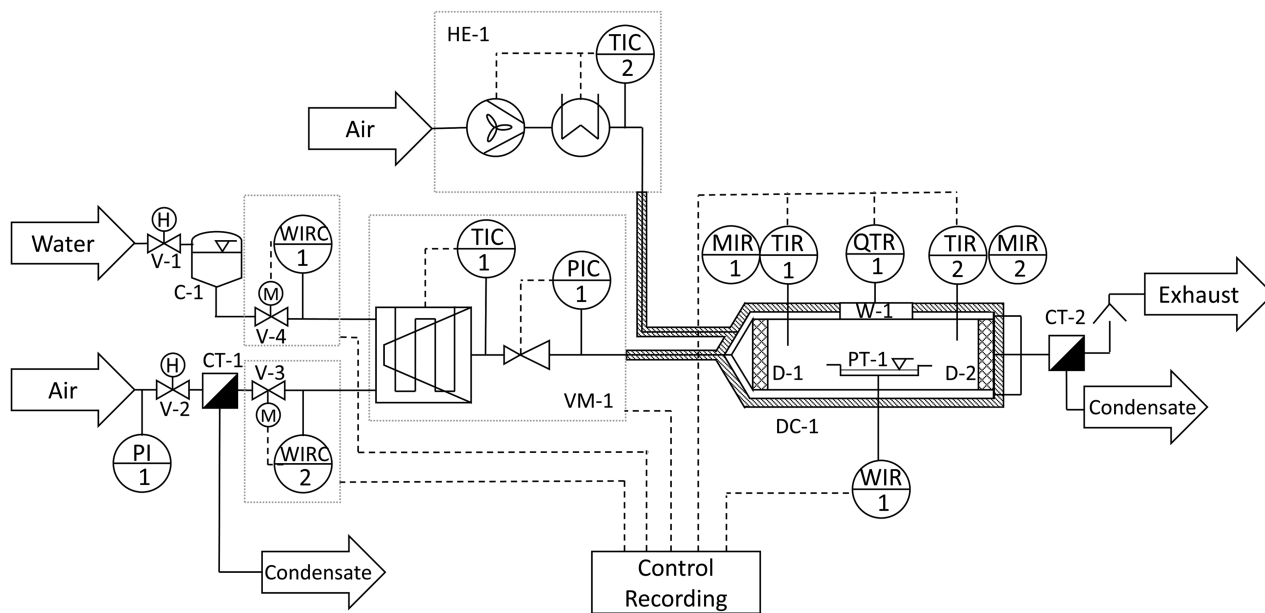


FIG. 4. Process flow diagram of the thin film drying device with air and water supply, air conditioning, and drying channel.

635-2; Testo SE & Co. KGaA; Germany). The sleeves are designed in such a way that the cross section of the channel remains unchanged during operation without humidity measurement. The control of temperature, humidity, air velocity, and the data acquisition with a selectable acquisition rate is implemented with a LabVIEW VI (LabVIEW 2019; National Instruments Corporation; Texas/USA).

III. EXPERIMENTAL

A. Method and measurement validation

After warm-up of the wind channel, the data recording is started, the airflow is shortly stopped to tare the balance (including the sample rack), and the empty sample platelet is weighted. After re-taring the rack (including platelet), the airflow is started to obtain the individual aerodynamic lift on the sample platelet and sample rack as averaged value (maximum observed values <2.1 mg) as there is a slight and random fluctuation of the balance value. This value is later taken into account to correct the gravimetric data. Finally, the platelet is taken out, and the sample is applied into the platelet cavity with a pipette and then inserted into the conditioned channel. For an initial sample mass of 1.7 g and water content of 1 g g⁻¹ db (see experimental data in Fig. 5), the cavity with an area of 25 cm² was milled to a depth of 250 μ m and 50 μ m for an initial water content of 9 g g⁻¹ db (see experimental data in Fig. 6).

To validate the online gravimetry of the drying experiments, a central aspect of the drying process characterization, each film is check-weighed after the experiment using a precision balance (Sartorius BCE224i-1S; Sartorius AG; Germany; reproducibility 0.1 mg) and the sample mass difference between external and online measurement is determined. The quotient of this mass difference and

the mass of the end product (check-weighing) is used as a percentage quality criterion as modulus, hereafter called “percentage error.” Any attempts with a percentage error greater than 0.5% were discarded. To avoid mass changes due to sorption after removal, the dried film is covered with aluminum foil before weighing.

B. Parameters of influence on drying rate

Maltose as the main component of malt extract is an industrially important sugar, which is not prone to crystallization during drying. It is, therefore, well suited for an exemplary investigation of the influence of the parameters air humidity, temperature, and air speed on the drying kinetics of a disaccharide, without obtaining an effect due to water release or uptake from crystallization. Maltose monohydrate (Merck KGaA; Germany) with 99% purity was dissolved in ultrapure water (Milli-Q; Merck KGaA; Germany) and left to stand for 12 h. The initial water content on dry basis was 1 g g⁻¹ db (dry basis). The experiments were conducted in duplicate, and the average value was plotted with error bars representing the maximum difference between the replicates. Figure 5 shows the influence on the drying rate of aqueous maltose solution by different temperatures (a), relative humidity (b), and flow rates (c). The maximum drying rate increases with the increasing temperature from 0.021 g g⁻¹ min⁻¹ at 25 °C to 0.091 g g⁻¹ min⁻¹ at 120 °C. With increasing humidity, the maximum drying rate decreases due to decreasing vapor pressure difference between the film surface and the air. At air humidity of 50% and 75% , a sharp initial peak in the drying rate can be observed, which can be explained by the fact that the introduction into the channel briefly reduces the humidity due to the entry of dry air from the surrounding insulation duct. Furthermore, it is interesting to note that for a relative humidity of 50% and higher, the constant rate period is extended in

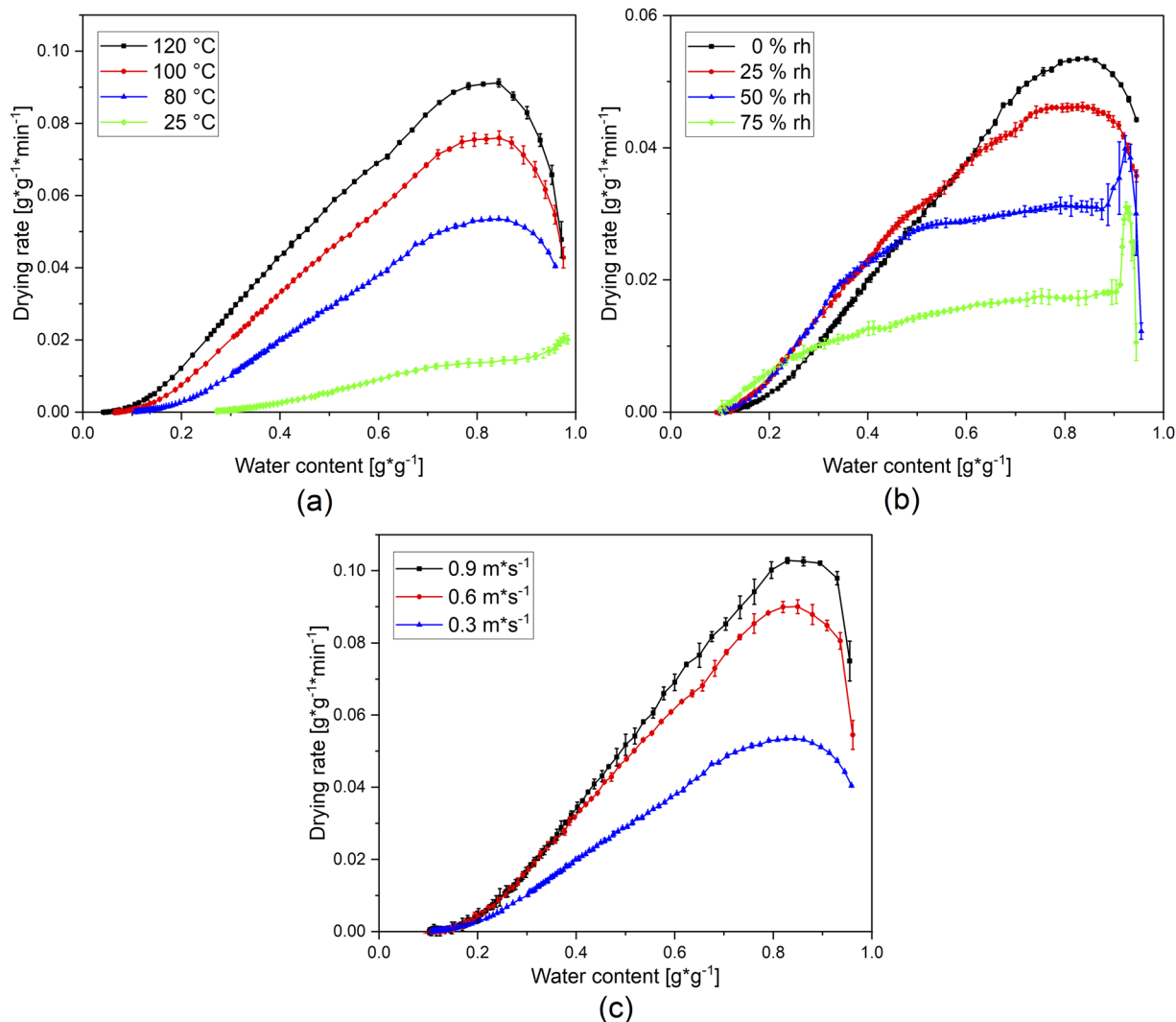


FIG. 5. Influence of temperature (a), relative humidity (b), and air velocity (c) on the drying rate of aqueous maltose solution with an initial water content of $1 \text{ g}^{-1} \text{ db}$ (dry basis), initial sample mass of 1.7 g , and sample area of 25 cm^2 . The constant parameters during variation were a temperature of $80 \text{ }^\circ\text{C}$, relative humidity of 0% , and an air velocity of 0.3 m s^{-1} .

comparison to the drying experiments with dry air and, after a certain time, the drying rates are above those at 0% humidity. This could be explained by skin formation on the surface under more severe drying conditions. The drying rate can also be varied well by changing the air velocity, but the difference between the drying rates at 0.3 and 0.6 m s^{-1} is much more pronounced than between 0.6 and 0.9 m s^{-1} . Drying of maltose solution at different temperatures leads to a percentage error of 0.16% with no detectable trend of temperature dependence (definition of “percentage error” in the previous chapter 3.1). The drying experiments with varying humidity at $80 \text{ }^\circ\text{C}$ showed a mean percentage error of 0.12% , also without detectable dependence regarding the air humidity level. Experiments with varying air velocity led to percentage errors of 0.13% , 0.12% , and 0.21%

for 0.3 , 0.6 , and 0.9 m s^{-1} , respectively, which denotes higher inaccuracies at elevated velocities. This is probably due to the increased formation of vortices behind the sample rack, which increases the gravimetric fluctuations and, thus, the inaccuracy.

C. Responsiveness of the drying rate to parameter changes

In order to illustrate the fast response of the setup and the drying rate to dynamic changes in temperature, humidity, and air velocity, further drying experiments were performed with maltose solution and a water content of $9 \text{ g}^{-1} \text{ db}$. A temperature step from 80 to $100 \text{ }^\circ\text{C}$ during the first drying stage, seen in Fig. 6(a) with dry

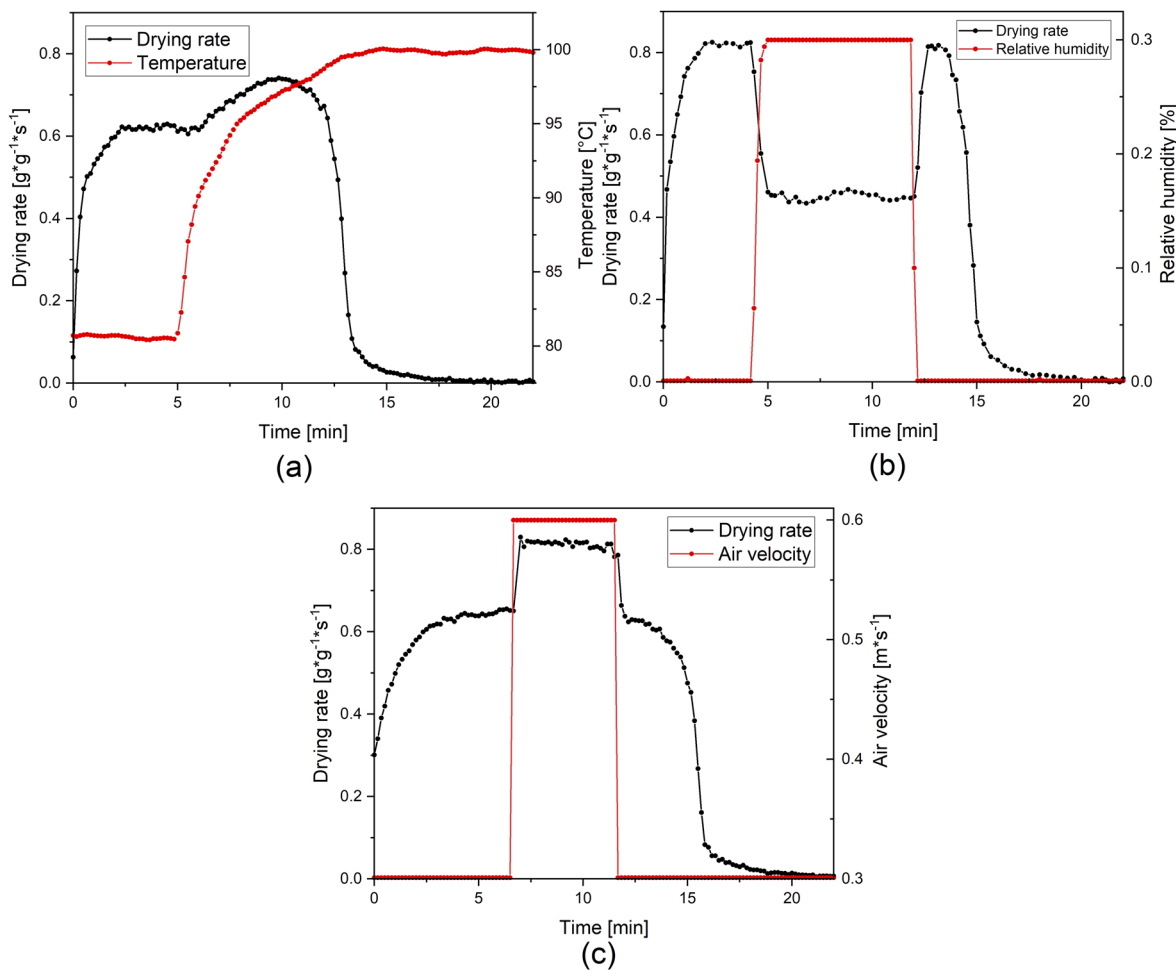


FIG. 6. Response of the drying rate to a temperature rise from 80 to 100 °C (a), to changes in relative humidity between 0% and 30% (b) and to changes in the air velocity between 0.3 and 0.6 m s⁻¹ (c). The remaining, constant parameters during variation were a temperature of 100 °C, a relative humidity of 0%, and an air velocity of 0.6 m s⁻¹. Maltose solution with an initial water content of 9 g g⁻¹ db was used.

air and an air velocity of 0.6 m s⁻¹, illustrates the corresponding change in the drying rate. The temperature was changed from 80 to 100 °C 5 min after the start of the experiment, whereupon the temperature increased by 85% relative to the desired 20 °C step within 5 min. Figure 6(b) exemplarily shows the response of the drying rate to a dynamic humidity change at a constant air temperature of 100 °C and air velocity of 0.6 m s⁻¹. The relative humidity was increased from 0% to 30% at 4 min after the experiment start and set back 8 min later (humidity pulse) resulting in a halving, respectively, doubling of the drying rate. The MFC reaches 85% of the setpoint mass flow 20 s after increase and drops to 0% after only 3 s. About 30–40 s after the parameter change, the drying rate changes to a new, constant value. The effect of changing the air velocity from 0.3 to 0.6 m s⁻¹ on the drying rate is shown in Fig. 6(c). The temperature of the dry air was held constant at 100 °C. The air velocity reaches the new setpoint within 3 s, and the drying rate changes within about 10 s from 0.64 to 0.81 g g⁻¹ min⁻¹ and back. In summary, it can be

stated that the drying parameters can be changed in a significantly shorter time span than the total drying time with a clear effect on the drying rate. This provides the basis for the control of kinetically coupled property changes during drying.

IV. CONCLUSION

This paper presents a thin film dryer concept for *in situ* drying manipulation, its constructive implementation, and the determination of the drying kinetics with high accuracy. It allows for the manipulation of the drying process via rapid changes in temperature, humidity, and air velocity. With the presented setup, the optical observation of coupled effects, e.g., *in situ* crystal formation and growth, morphology, or degradation, is possible. For the first time, the new setup enables the *in situ* manipulation and simultaneous observation of product property changes such as crystallization or degradation. It, therefore, extends the classical measurement

and operating techniques that are restricted to constant drying conditions with post-experimental property analysis.

The result of the design is a double-walled wind channel with gas conditioning in which measurement and control technology (thermocouples, IR thermometers, and humidity sensors) are integrated and can be modified easily. The gas conditioning consists of two mass control valves for water and dehumidified air, which supply a combined evaporator-mixer unit with defined material flows. The drying channel itself is surrounded by an isolation channel, which can be fed with tempered air (according to the test conditions) to ensure a quick response to the required process conditions in the wind channel. With this concept, drying and drying rate manipulation is possible up to a temperature of 200 °C with the aid of vapor or vapor-air mixtures at water mass flows of up to 1200 g h⁻¹ or air velocities of up to 1.5 m s⁻¹. The function of the setup was validated, a measurement methodology for increased accuracy was presented, and the influence of the variable drying conditions (air speed, temperature, and humidity) on the drying kinetics was demonstrated using maltose solution as a model. Furthermore, the high degree of the setup's dynamics was demonstrated by *in situ* changes in the drying parameters and their effects on the drying rate.

The described experimental setup is, therefore, a powerful instrument with the perspective to accurately estimate the effects of process parameters already during the drying process. The main benefit of this setup is the possibility to manipulate the drying process regarding temperature, relative humidity, and velocity in a very wide range and highly dynamic manner. The fully equipped setup allows the direct visualization of optical detectable effects (morphology, crystallization growth, and nucleation) coupled to these parameter changes. With the real-time adaption of the drying process, the setup, thus, opens up the possibility for the control of the formation of specific product properties, which is considered to have great potential for future applications in research and industry.

SUPPLEMENTARY MATERIAL

See the [supplementary material](#) for the constructive details of the main parts (technical drawings) and an image of the setup.

ACKNOWLEDGMENTS

We sincerely thank the students Matthias Kilger and Bianca Wegert-Raisig for their great support during construction and experimental work. Furthermore, we acknowledge the Deutsche Forschungsgemeinschaft (DFG) for the funding of Project No. Fo 357-3-1.

AUTHOR DECLARATIONS

Conflict of Interest

The authors have no conflicts to disclose.

DATA AVAILABILITY

The data that support the findings of this study are available within the article and its [supplementary material](#) and are available from the corresponding author upon reasonable request.

REFERENCES

- 1 D. Das, H. A. Husni, and T. A. G. Langrish, "The effects of operating conditions on lactose crystallization in a pilot-scale spray dryer," *J. Food Eng.* **100**(3), 551–556 (2010).
- 2 I. Schmitz-Schug, P. Foerst, and U. Kulozik, "Impact of the spray drying conditions and residence time distribution on lysine loss in spray dried infant formula," *Dairy Sci. Technol.* **93**, 443 (2013).
- 3 I. Schmitz-Schug, U. Kulozik, and P. Foerst, "Modeling spray drying of dairy products—Impact of drying kinetics, reaction kinetics and spray drying conditions on lysine loss," *Chem. Eng. Sci.* **141**, 315–329 (2016).
- 4 M. A. I. Schutyser, E. M. Both, I. Siemons, E. M. J. Vaessen *et al.*, "Gaining insight on spray drying behavior of foods via single droplet drying analyses," *Drying Technol.* **37**(5), 525–534 (2019).
- 5 W. Liu, W. D. Wu, C. Selomulya, and X. D. Chen, "Assembly of pharmaceutical microparticles via spray drying," in *18th International Drying Symposium IDS 2012: Conference Proceedings* (18th International Drying Symposium (IDS2012), Xiamen, 2012).
- 6 E. M. Both, R. M. Boom, and M. A. I. Schutyser, "Particle morphology and powder properties during spray drying of maltodextrin and whey protein mixtures," *Powder Technol.* **363**, 519–524 (2020).
- 7 M. O. Wittner, H. P. Karbstein, and V. Gaukel, "Energy efficient spray drying by increased feed dry matter content: Investigations on the applicability of air-core-liquid-ring atomization on pilot scale," *Drying Technol.* **38**(10), 1323–1331 (2020).
- 8 I. Schmitz-Schug, U. Kulozik, and P. Foerst, "Reaction kinetics of lysine loss in a model dairy formulation as related to the physical state," *Food Bioprocess Technol.* **7**, 877 (2013).
- 9 D. Das and T. A. G. Langrish, "Combined crystallization and drying in a pilot-scale spray dryer," *Drying Technol.* **30**(9), 998–1007 (2012).
- 10 A. Ibach, *Verminderung der Verbackungsneigung von Sprühtrockneten Laktosehaltigen Pulvern* (Univ.-Verl. Karlsruhe, Karlsruhe, 2007), ISBN: 978-3-86644-172-9.
- 11 M. Hartmann and S. Palzer, "Caking of amorphous powders—Material aspects, modelling and applications," *Powder Technol.* **206**(1–2), 112–121 (2011).
- 12 C. Chen, C. Venkatasamy, W. Zhang, L. Deng *et al.*, "Effect of step-down temperature drying on energy consumption and product quality of walnuts," *J. Food Eng.* **285**(8), 110105 (2020).
- 13 M. W. Woo, M. G. Lee, S. Shakiba, and S. Mansouri, "Controlling *in situ* crystallization of pharmaceutical particles within the spray dryer," *Expert Opin. Drug Delivery* **14**(11), 1315–1324 (2017).
- 14 C. L. Har, N. Fu, E. S. Chan, B. T. Tey *et al.*, "Unraveling the droplet drying characteristics of crystallization-prone mannitol—Experiments and modeling," *AIChE J.* **63**(6), 1839–1852 (2017).
- 15 M. W. Woo, N. Fu, F. T. Moo, and X. D. Chen, "Unveiling the mechanism of *in situ* crystallization in the spray drying of sugars," *Ind. Eng. Chem. Res.* **51**(36), 11791–11802 (2012).
- 16 S. Shakiba, S. Mansouri, C. Selomulya, and M. W. Woo, "The role of the intermediate stage of drying on particle *in-situ* crystallization in spray dryers," *Powder Technol.* **323**(6), 357–366 (2018).
- 17 S. Shakiba, S. Mansouri, C. Selomulya, and M. W. Woo, "In-situ crystallization of particles in a counter-current spray dryer," *Adv. Powder Technol.* **27**(6), 2299–2307 (2016).
- 18 D. H. Charlesworth and W. R. Marshall, "Evaporation from drops containing dissolved solids," *AIChE J.* **6**(1), 9–23 (1960).
- 19 T. T. H. Tran, J. G. Avila-Acevedo, and E. Tsotsas, "Enhanced methods for experimental investigation of single droplet drying kinetics and application to lactose/water," *Drying Technol.* **34**(10), 1185–1195 (2016).
- 20 E. M. Both, A. M. Karlina, R. M. Boom, and M. A. I. Schutyser, "Morphology development during sessile single droplet drying of mixed maltodextrin and whey protein solutions," *Food Hydrocolloids* **75**(2), 202–210 (2018).
- 21 J. Perdana, M. B. Fox, M. A. I. Schutyser, and R. M. Boom, "Single-droplet experimentation on spray drying: Evaporation of a sessile droplet," *Chem. Eng. Technol.* **34**(7), 1151–1158 (2011).
- 22 R. Büttiker, "Mechanismus der partikelformung bei der trocknung freifallender, feststoffhaltiger tropfen," *Chem. Ing. Tech.* **53**(4), 280–281 (1981).

- ²³D. A. Wallack, T. M. El-Sayed, and C. J. King, "Changes in particle morphology during drying of drops of carbohydrate solutions and food liquids. 2. Effects of drying rate," *Ind. Eng. Chem. Res.* **29**(12), 2354–2357 (1990).
- ²⁴C. Groenewold, "Determination of single-particle drying kinetics in an acoustic levitator," *Chem. Eng. J.* **86**(1–2), 217–222 (2002).
- ²⁵J.-M. Schweitzer, M. Serval, F. Salvatori, A. Dandeu *et al.*, "Spray drying of colloidal suspensions: Coupling of particle drying and transport models with experimental validations," *Chem. Eng. Res. Des.* **170**(8), 224–238 (2021).
- ²⁶J. Perdana, R. G. M. van der Sman, M. B. Fox, R. M. Boom, M. A. I. Schutyser *et al.*, "Measuring and modelling of diffusivities in carbohydrate-rich matrices during thin film drying," *J. Food Eng.* **122**, 38–47 (2014).
- ²⁷F. Gómez-Narváez, "Design and construction of a thin-film drying channel equipment—Modeling the drying kinetics of nanofiltered whey," *J. Food Eng.* **263**, 359–365 (2019).
- ²⁸M. Räderer, A. Besson, and K. Sommer, "A thin film dryer approach for the determination of water diffusion coefficients in viscous products," *Chem. Eng. J.* **86**(1–2), 185–191 (2002).
- ²⁹M. Mueller, P. Scharfer, M. Kind, and W. Schabel, "Determination of diffusion coefficients of non-volatile additives in polymeric coatings by means of inverse micro Raman spectroscopy," *Chem. Ing. Tech.* **82**(12), 2097–2102 (2010).
- ³⁰X. Y. Li, I. Zbicinski, and W. Jing, "A scaling-up approach from experimental tunnel to spray dryer," *Int. J. Food Eng.* **6**(1) (2010).
- ³¹E. M. Both, S. M. B. Tersteeg, R. M. Boom, and M. A. I. Schutyser, "Drying kinetics and viscoelastic properties of concentrated thin films as a model system for spray drying," *Colloids Surf., A* **585**, 124075 (2020).
- ³²B. Adhikari, T. Howes, A. K. Shrestha, W. Tsai *et al.*, "Thin-layer isothermal drying of fructose, maltodextrin, and their mixture solutions," *Drying Technol.* **24**(11), 1415–1424 (2006).